Journal of Thermal Biology 83 (2019) 119–133

Contents lists available at ScienceDirect

Journal of Thermal Biology

journal homepage: www.elsevier.com/locate/jtherbio

A numerical study on thermal ablation of brain tumor with intraoperative focused ultrasound

Amir Abdolhosseinzadeh, Afsaneh Mojra*, Ali Ashrafizadeh

Department of Mechanical Engineering, K. N. Toosi University of Technology, Tehran, Iran

ARTICLE INFO

Keywords:
Focused ultrasound surgery (*FUS*)
Brain tumor
Tumor ablation
Bio-heat transfer
Finite element method

ABSTRACT

Focused ultrasound surgery (*FUS*) is a non-invasive thermal therapeutic method which has been emerged in the field of brain tumors treatment. During intraoperative brain surgery, application of *FUS* can significantly increase the accuracy of thermal ablation of tumor while reducing undesirable damage to healthy brain tissue. The main objective of this study is acquiring acoustic transducer specifications to achieve optimum thermal treatment in the tumoral tissue. *2D* and *3D* models are constructed from patient-specific brain *MRI* images which consist of a malignant vascular tumor. Acoustic pressure and temperature are obtained by using homogenous Helmholtz and bio-heat transfer equations according to insignificant nonlinear effect. Besides that, thermal lesion induced by *FUS* is obtained by the thermal dose function. Results show the significance of blood vessels' cooling effect on the temperature profile. Moreover, correlation between temperature profile and transducer's operating parameter including power, frequency and duty cycle is obtained. Artificial neural network analysis is conducted to estimate required transducer parameters for optimum temperature rise.

1. Introduction

Utilization of Focused Ultrasounds Surgery *(FUS)* beams has become one of the developing methods of cancer treatment due to its low side effects (ter Haar, 2016). The target of this method is to raise temperature solely within the focal area for the purpose of acquiring demanded thermal damage while minimizing the undesirable damage to the adjacent tissues. The volume of the damaged area depends on the adjustment of *FUS* system and mechanical properties of the target tissue. Assessing the temperature field in the focal area is essential to guarantee the clinical output and patient tranquility.

FUS has many curative applications in medical science (Amini, 2018; Escoffre and Bouakaz, 2015; Guan and Xu, 2016; Peek et al., 2015; Sofuni et al., 2014). Over the past years, numerous studies have been done on the simulation of ultrasound wave propagation in cancerous tissues to induce optimal temperature increase (Almekkaway et al., 2017; Okita et al., 2010). Solovchuk et al. (2014) probed the relation between prognosticated temperature increase and experimental temperature increase. In order to obtain experimental temperature increase, a porcine muscle was used. The tissue was heated through focused ultrasound waves for 30s. It was concluded that for temperatures below 85–90 °C, there is good agreement between the simulation results and experimental data. The main drawback of these studies is neglecting the cooling effect of blood vessels.

Tumor is abnormal cell proliferation in the tissue. According to the pathological findings, tumor growth has two distinct phases which are the avascular phase and the vascular phase. During the avascular phase of tumor growth, a limited number of cancer cells aggregates in the healthy tissue. In the experimental models, maximum tumor size in the avascular phase is considered 1–2 mm (Folkman, 1990). The next stage of the tumor growth is the vascular phase in which new blood vessels are recruited to nourish the increased number of cancer cells (Mascheroni et al., 2016). It is affirmed that by the time a tumor is approximately 2-3 mm, it will contain more than 1 million cells and it has already entered the vascular phase of growth (Weidner et al., 1991).

Numerical and experimental studies on the effect of blood vessels on temperature distribution in *FU* (Focused Ultrasound) therapy indicated that the temperature rise with and without considering blood vessels has significant difference (Hariharan et al., 2007; Solovchuk et al., 2012; Zhang et al., 2006). Huang et al. (2004) modeled nonlinear propagation of ultrasound wave in a thermo-viscous domain. They observed that in the presence of blood flow and acoustic streaming induced by *FU*, temperature rise would diminish near the large blood vessel. They concluded that by preventing or decreasing the blood flow into the tumoral domain, the efficiency of hyperthermia treatment

* Corresponding author. Department of Mechanical Engineering, K. N. Toosi University of Technology, 15 Pardis St., Tehran, 1991943344, Iran.
E-mail address: mojra@kntu.ac.ir (A. Mojra).

https://doi.org/10.1016/j.jtherbio.2019.05.019
Received 16 January 2019; Received in revised form 13 May 2019; Accepted 19 May 2019
Available online 23 May 2019

would increase. A model of blood vessel network was used by Huang et al. (2010) to numerically obtain tissue temperature near the focal area. They concluded that size of the blood vessels is an important factor on power absorption by the tumor. Considering the significance of blood vessels effect on the temperature profile, inclusion of the real geometry of blood vessels in the numerical simulation is necessary. This has been underestimated in most of the previous studies.

In addition to the geometry of blood vessels, rate of blood perfusion, mechanical and thermo-physical properties and geometrical features of the tumoral tissue, and the transducer operating parameters affect the efficiency of ultrasound hyperthermia (Billard et al., 1990; Samanipour et al., 2013). The effect of using nanoparticles on the temperature rise was studied for in vivo and in vitro CT26 tumors (Beik et al., 2016). Results of this study revealed that using nanoparticles accompanied by the sound waves, reduces the exposure time significantly. Effect of the specific heat capacity and thermal conductivity of the tissue on the damaged area was investigated by Guntur et al. (2015). They concluded that the mentioned thermo-physical properties have significant effect on temperature distribution near the focal area. Huang et al. (2015) used a three-dimensional model to study the effect of dynamic change of material properties as a result of *FU* application on the temperature field. They concluded that at low powers of *FU* without the creation of bubbles, there is a good agreement between numerical and experimental results.

By taking into account various influential parameters on the *FUS*, several studies have been conducted to optimize the treatment (De Greef et al., 2010; Kok et al., 2013; Siauve et al., 2004). Optimization of ultrasound parameters in order to get effective drug delivery was investigated by Wang et al. (2011). The optimization variables included acoustic power, pulse repetition frequency and duty cycle, and optimum treatment was based on an experimental study which was done by Dromi et al. (2007). In the study by Gholami et al. (2017), the transducer operating parameters including the frequency and the input power, were determined to obtain the optimum thermal dose function, numerically. Frequency values of 2, 3, 4 and 5 MHz with the input powers of 50 and 100W were examined and maximum thermal dose was observed in the tissue domain at the frequency of 2 MHz and input power of 100W. This result provided the possibility of short treatment time for a large tumoral tissue. Kok et al. (2017) developed a software package suitable for diverse applications of hyperthermia with *FU*. The software package was tested by using a model of pancreas cancer in the vascular phase.

In this study, *FUS* is used for thermal necrosis of a brain tumor. The objective is to optimize the transducer operating parameters including the ultrasound power, frequency, and the duty cycle, by studying the temperature field in the tumoral tissue through the thermal dose function in order to reach the optimum *FU* thermal treatment. The *FUS* is established intraoperatively which contains removing a section of skull to locate the ultrasound transducer. A transducer is placed above the brain to focus the ultrasound beams in the area of tumoral tissue with the aim of minimizing damage to the healthy regions. A bowl-shaped transducer is employed to generate focused beams. Brain tissue geometry is acquired from patient-specific *MRI* images which includes a malignant tumor in the vascular phase of growth. In order to determine the temperature distribution in the focal area, the homogeneous Helmholtz and the bio-heat transfer equations need to be solved. The numerical prognostication allows users to study the thermal lesion induced by *FUS* when varying input parameters of the transducer.

2. Material and methods

2.1. Problem definition

In order to apply *FU* treatment intraoperatively, a small section of the skull is removed to locate the ultrasound transducer on the brain surface above the tumor. For the numerical simulation, a three-dimensional geometry of the brain tissue including a malignant tumor is constructed by using patient-specific *MRI* images. All procedures followed are in accordance with the ethical standards of the responsible committee on human experimentation (institutional and national) and with the Helsinki Declaration of 1975, as revised in 2000 (5). Informed consent is obtained from the patient for being included in the study.

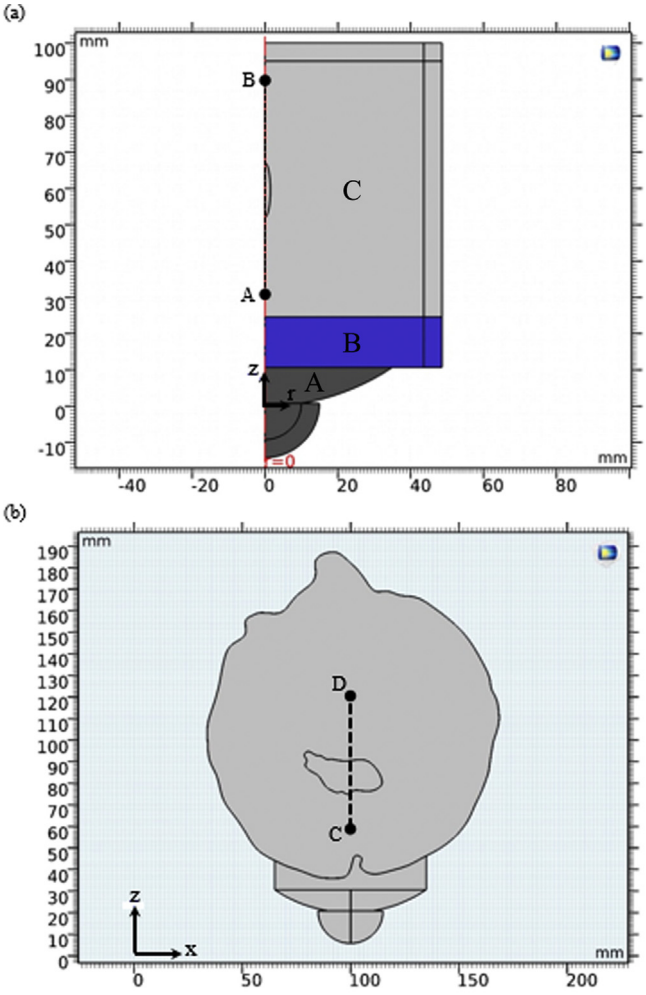

Fig. 1. (a) Geometry of the transducer (domain A), water (domain B) and tissue section (domain C) in the *2DNT* model, path A-B is defined; (b) real geometry of the *2D* brain model, path C-D is defined.

Table 1
Geometrical characteristics of transducer (Huang et al., 2004).

Parameter	Dimension (mm)
Focal length	62.64
Aperture	70
Hole	10

The homogeneous Helmholtz and bio-heat transfer equations are linked together to acquire the acoustic pressure and the temperature profile in the tumoral tissue. Nonlinear effect of wave propagation is studied and neglected according to the small differences between the linear and nonlinear results at low transducer powers. Subsequently, cooling effect of blood vessels is considered by adding microvessels to the tumor. In order to afford the excessive computational costs, two-dimensional model of the brain tissue including a tumor in the vascular phase of growth is constructed by using a cross-section of *MRI* images. The *FU* application for thermal treatment is optimized for the *2D* model

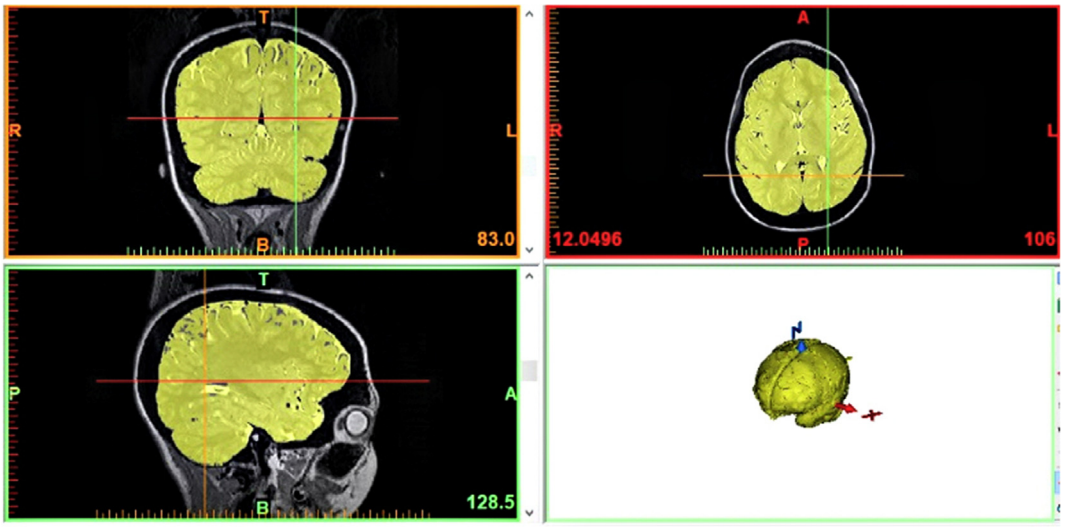

Fig. 2. Different views of the brain tissue, top left: coronal view, top right: axial view, bottom left: sagittal view, bottom right: isometric.

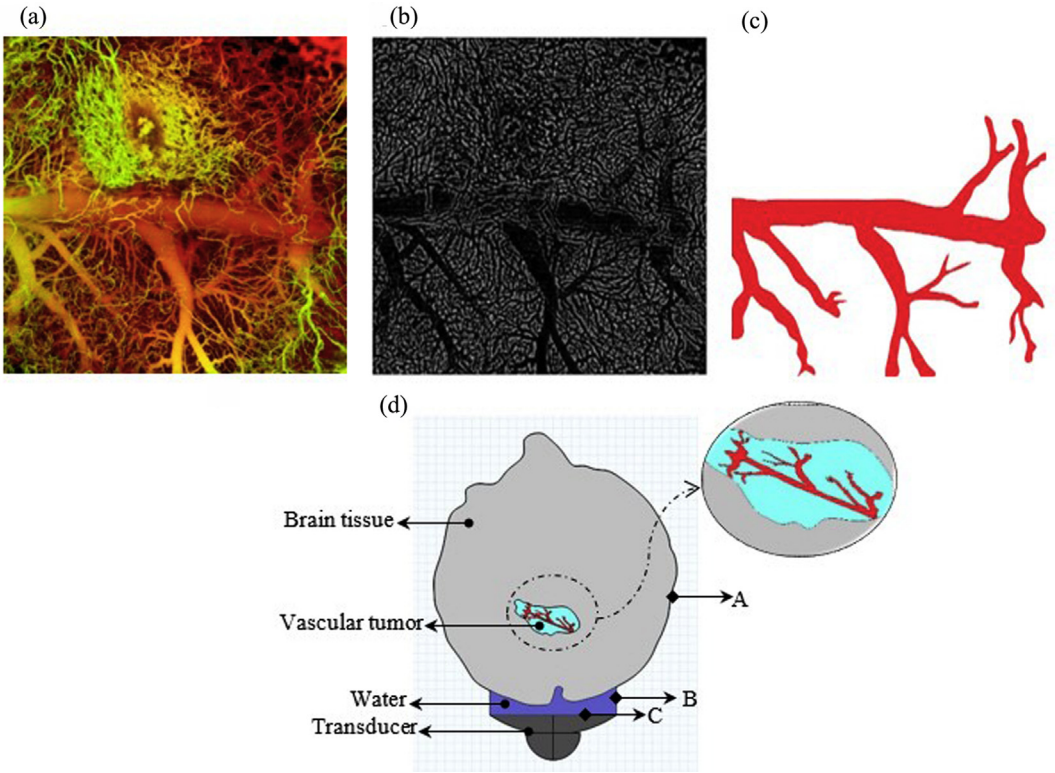

Fig. 3. (a) Network of the blood vessels inside Glioblastoma (K. I. P. Galleries), (b) blood vessels' model after segmentation, (c) final geometry of blood vessels inside the tumoral region, (d) 2D geometry of the brain tissue including a malignant tumor in the vascular phase, referred to as *2DVT* model, A, B, and C are used to define boundary conditions.

versus the power of transducer, frequency and duty cycle of the pulse wave propagation as design variables, to obtain maximum temperature rise in the tumoral region. The optimization procedure is performed by employing a feed forward artificial neural network.

2.2. Governing equations

For the simulation of ultrasound wave propagation inside the brain and tumoral tissues, the homogeneous Helmholtz equation is employed. In order to evaluate the nonlinear effects of wave propagation, *HIFU* (High Intensity Focused Ultrasound) simulator is used to obtain the absolute pressure by employing the nonlinear *KZK* (Khokhlov-Zabolotskaya-Kuznetsov) equation for wave propagation. *HIFU* simulator is a MATLAB code through which ultrasound wave propagation is simulated based on *KZK* equation. Results are compared with the results of linear Helmholtz equation. Based on this comparison which is provided in section 3.1, nonlinear effects are neglected. Homogeneous Helmholtz equation for acoustic wave propagation with specified frequency in the tissue is described by Eqs. (1)–(3):

$$\nabla.\left(-\frac{1}{\rho_c}(\nabla p_t - q_d)\right) - \frac{k_{eq}^2 p_t}{\rho_c} = Q_m \tag{1}$$

$$p_t = p + p_b \tag{2}$$

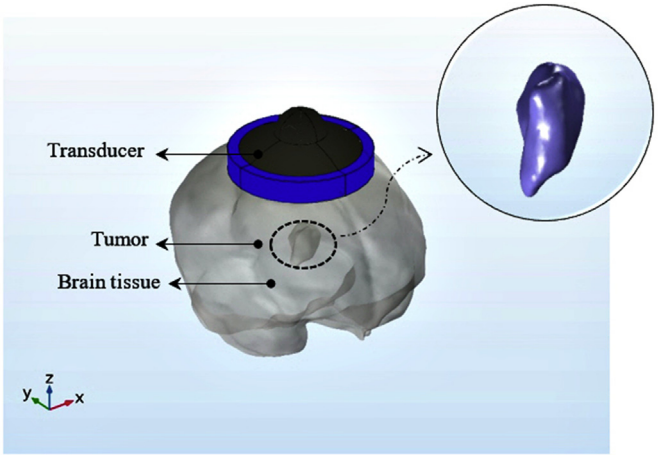

Fig. 4. *3D* geometry of the brain tissue including a malignant tumor, referred to as *3DST* model.

$$k_{eq}^2 = \left(\frac{\omega}{c_c}\right)^2 - \left(\frac{m}{r}\right)^2 \tag{3}$$

where ρ_c is the tissue density, p_t is the total pressure, q_d is the volumetric force, k_{eq} is the wave number, Q_m is a domain heat source causing pressure variations, p and p_b are scattered pressure and background pressure respectively, ω is the angular frequency, C_c is the speed of sound in the medium, m is a circumferential mode number and r represents the radius. Q_m is neglected in this equation.

The displacement amplitude applied by the ultrasound transducer has direct correlation with the ultrasound power. Equation (4) describes the relation between normal displacement, wave intensity and power of the transducer as follows:

$$P = \frac{I}{A} = \frac{\xi^2 \omega^2 Z}{A} \tag{4}$$

where P is the power of transducer, I is the ultrasound wave intensity, ξ is the displacement amplitude of transducer, Z is the acoustic impedance of the medium through which the wave is propagated and A is the surface area of the transducer head.

Following the solution of the Helmholtz equation, the generated heat, which is the heat source for subsequent thermal analysis, is obtained using Eq. (5):

$$Q = 2\alpha_{ABS} I = 2\alpha_{ABS} \left| Re\left(\frac{1}{2} pv\right) \right| \tag{5}$$

where α_{ABS} is the acoustic absorption coefficient of the medium, and v is the acoustic particle velocity vector.

Considering the ultrasound heating as a heat source, heat transfer in the brain tissue can be described by the Pennes bio-heat transfer equation (Pennes, 1998) (Eq. (6)) as follows:

Table 3
Material properties used in the *FUS* simulation (Duck, 1990; Yacoob and Hassan, 2012).

Analysis	Parameter	Water	Brain tissue	Tumor	Blood
Pressure Acoustics	Density $\left(\frac{Kg}{m^3}\right)$	1000	1060	1043	1055
	Speed of sound $\left(\frac{m}{s}\right)$	1483	1590	1612	1575
Thermal	Attenuation coefficient $\left(\frac{dB}{m}\right)$	0.217	80	80	0.217
	Thermal conductivity $\left(\frac{W}{m.K}\right)$	–	0.535	0.5	0.52
	Heat capacity at constant pressure $\left(\frac{J}{Kg.K}\right)$	–	3650	3621	3490

$$\rho_c C_p \frac{\partial T}{\partial t} = \nabla.(K\nabla T) - \rho_b C_b \omega_b (T - T_b) + Q + Q_{met} \tag{6}$$

where T is the temperature, ρ_c, k and C_p represent density, thermal conductivity and specific heat of the tissue, respectively. ρ_b, C_b, ω_b, and T_b represent density, specific heat, blood perfusion rate, and temperature of the blood, respectively. Q is the ultrasound heating (the absorbed ultrasound energy calculated by Eq. (5)), and Q_{met} is the metabolic heat source. In this study, effect of blood perfusion and metabolic heat source are neglected.

Tumor and tissue damages as a result of ultrasound heating are evaluated by the thermal dose, relative to the temperature of 43 °C, indicated by Sapareto and Dewey, (1984). To cause thermal damage to the tissue, an equivalent heating period of 240 min at 43 °C is required. Increasing the temperature can reach an equivalent dose over much shorter time periods. The thermal dose function is given by Eq. (7) as follows:

$$D(x, y) = \frac{\sum_{t_0}^{t_{final}} R^{T_r - T(x,y,t)} \Delta t}{3600} \tag{7}$$

where, T_r is 43 °C, R is equal to 0.25 for $T < T_r$ and is equal to 0.5 for $T \geq T_r$.

2.3. Geometry construction

For *FUS* simulation, three distinct geometries are constructed as follows:

1. Model *2DNT*: A two-dimensional model with simplified geometry of the brain tissue without tumor used for validation;
2. Model *2DVT*: A two-dimensional model of real brain tissue including a tumor with microvessels inside the tumor constructed from patient-specific MRI images;
3. Model *3DST*: A three-dimensional model of real brain tissue including a tumor without microvessels to avoid excessive

Table 2
Details of governing equation for each boundary condition.

Analysis	Type of boundary	Equation	Details
Pressure Acoustics	Sound hard wall	$-n.\left(-\frac{1}{\rho_c}(\nabla p_t - q_d)\right) = 0$	n is normal vector
	Normal displacement (C)	–	1-5 (nm)
	Impedance1 (A)	$-n.\left(-\frac{1}{\rho_c}(\nabla p_t - q_d)\right) = -p_t \frac{i\omega}{Z_i}$	$Z_i = \rho_{water} \times C_{water}\rho_{water} = 1\frac{Kg}{m^3}$, $C_{water} = 1483\frac{m}{s}$
	Impedance2 (B)	$-n.\left(-\frac{1}{\rho_c}(\nabla p_t - q_d)\right) = -p_t \frac{i\omega}{Z_i}$	$Z_i = \rho_{air} \times C_{air}\rho_{air} = 1.2\frac{Kg}{m^3}$, $C_{air} = 343\frac{m}{s}$
Thermal	Constant temperature (A and B)	–	310.15 K

Table 4
Details of the applied mesh in the pressure acoustics and thermal analyses.

Model		*2DVT*				*3DST*	
Frequency		1 MHz		3 MHz		1 MHz	
Study		Acoustics	Thermal	Acoustics	Thermal	Acoustics	Thermal
Number of elements	Tetrahedral	–	–	–	–	1,006,498	2,148,667
	Triangular	394,035	238,312	2,878,751	494,808	40,571	44,066
Number of nodes		197,784	119,773	1,441,459	248,021	173,629	358,959

computational costs, constructed from patient-specific *MRI* images.

Fig. 1a demonstrates the first model (*2DNT*) which is used for validation of the *FUS* simulation. As can be seen in Fig. 1a, the model has axial symmetry and includes of three domains; the transducer (domain A), the water (domain B) and tissue section (domain C). Geometrical characteristics of the transducer used for the *FUS* simulation are listed in Table 1.

Real *2D* geometry of the brain tissue is displayed in Fig. 1b. In order to construct this geometry, *MRI* images of a male patient with a malignant brain tumor are used based on the Helsinki agreement. Fig. 2 shows different views of the brain tissue in three planes of axial, coronal, sagittal and also isometric view.

The *MRI* images are imported to Mimics Medical software (version 19, Materialise NV, Leuven, Belgium). Then by Materialise 3-matic Medical software (version 11, Materialise NV, Leuven, Belgium), an appropriate file is provided to import the geometry into the COMSOL Multiphysics software (version 5.3, COMSOL Inc., Burlington, MA).

The model of the microvessels inside a Glioblastoma is obtained from an image provided by Koch Institute Public Galleries (Galleries, 2013) (Fig. 3a). In order to extract blood vessels, MATLAB (version R2016a, MathWorks, Natick, Massachusetts, United States) image processing is used. After applying blood vessel segmentation, the processed image is produced which is shown in Fig. 3b. Glioblastoma is the most aggressive cancer of the brain. Final geometry of the blood vessels inside the tumoral region is demonstrated in Fig. 3c.

Fig. 3d presents the geometry of second model (*2DVT*) which is a two-dimensional model of the brain tissue containing a Glioblastoma tumor with the blood vessels and the transducer located above the tumoral region. This model is constructed by a patient-specific cross-section of the *MRI* images.

An exact three-dimensional model of the brain tissue containing a Glioblastoma tumor is provided in Fig. 4. In this model, the blood vessels are neglected to reduce the prohibitive computational costs. For the purpose of considering blood vessels in *3D* simulation, computational elements with smaller size should be employed in the area of blood vessels. The required memory for such computational domain is over 42 GB in order to run both acoustic and thermal studies. In addition, *2D* geometry of blood vessels is extracted from Koch Institute Public Galleries by using MATLAB image processing tool. For *3D* simulation of blood vessels within Glioblastoma tumor, a micro-*CT* is essential which is out of access in this research. In spite of the computational cost hurdle as well as lack of reliable data, which justify the omission of the vascular structure in the *3D* model, it should be noted that this is an erroneous assumption. Therefore, the relevant error, which manifests itself in the computed temperature rise, should be estimated.

For *FUS* simulation, the transducer is located on the brain tissue above the tumoral region.

2.4. Boundary conditions and initial values

According to the ultrasound hyperthermia treatment procedure, two sets of boundary conditions should be defined. The boundaries are indicated in Fig. 3d. The first set of boundary conditions is needed for the pressure acoustics analysis. In this regard, the exterior boundaries of brain tissue and transducer (A and B) are in contact with the cerebrospinal fluid and air, respectively. Normal displacement amplitude is defined for contact surface of the transducer and the tissue (C). Other boundaries are defined as the sound hard wall which means that the normal component of acceleration for the sound waves is zero. The second set of boundary conditions is related to the thermal analysis for which the exterior boundary of brain tissue is defined to have constant temperature of the human body. Initial temperature of 310.15 K is considered for the whole brain tissue. Moreover, as it was mentioned above, a heat source is defined in the whole domain which would be deduced from the pressure acoustics study. The governing equations at the boundaries are provided in Table 2.

2.5. Material properties, mesh generation and computational algorithm

COMSOL multi-physics software is used to run the pressure acoustics and thermal analyses. Material properties used in this study are presented in Table 3.

For the pressure acoustics study, the grid should resolve the ultrasound wavelength. According to (Sklar, 1988), 4 elements per wavelength are sufficient. In the focused domain, a grid with the element size equal to $\frac{\lambda}{6} = 0.26$ mm (λ is the wavelength) is used. For *2D* and *3D* simulations, triangular and tetrahedral elements are used, respectively. Table 4 provides details of the applied mesh in both pressure acoustics and thermal analyses.

Duty cycle is the fraction of a complete cycle in which the transducer is activated, i.e. the duty cycle of a constant wave is equal to 1. In order to acquire optimum treatment, transducer operating time within a certain period should be considered. For the optimization problem, effects of the frequency, duty cycle, and the power of transducer are studied. Two frequencies of 1 MHz and 3 MHz are applied by the transducer to the normal and tumoral tissues. The frequency is applied by 3 different duty cycles which are 0.7, 0.8 and 1. To investigate the effect of transducer power, normal displacement amplitude of transducer is varied between 1 nm to 5 nm with steps of 1 nm. Moreover, the effect of pulse wave is investigated by 3 different duty cycles of 0.7, 0.8 and 1. Fig. 5 displays schematic of the waveform for the pulse wave propagation with the duty cycle of 0.7. The angular frequency of $4\pi\frac{rad}{s}$ is considered.

The pressure acoustics analysis is conducted in the steady state while the thermal analysis is a transient procedure with a time step of 0.1s. Ultrasound exposure time is assumed to be 10s in the thermal study.

The *FUS* simulations are carried out by using a system with 32-core *CPU* and 42 GB RAM. The computational times for *2D* and *3D* simulations are 39 min and 87 min, respectively.

A flowchart of the numerical procedure is illustrated in Fig. 6. The stopping criterion is obtaining the desired temperature rise in the tumoral tissue.

Input values for each of three mentioned models are listed in Table 5.

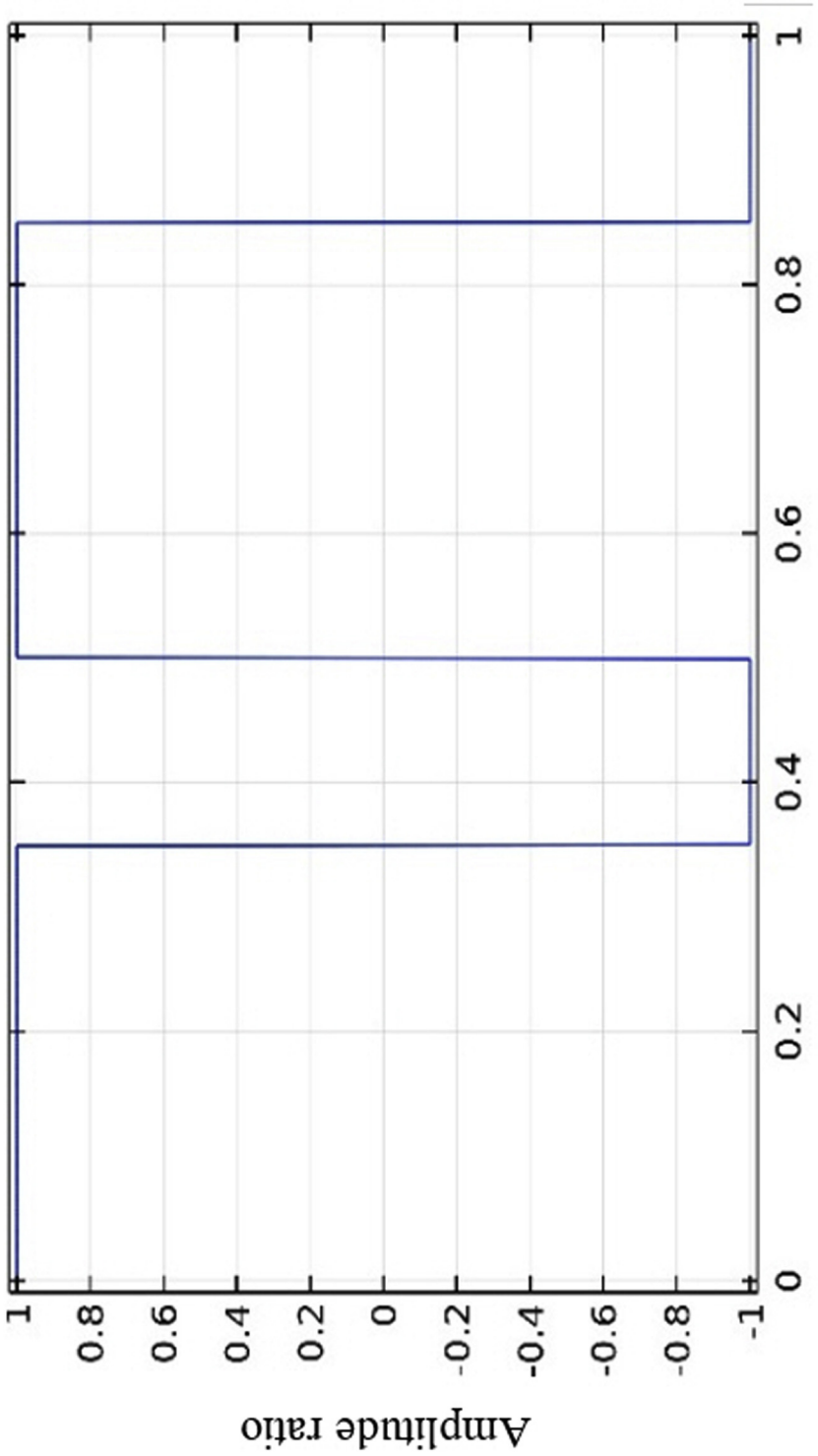

Fig. 5. Pulse wave with duty cycle of 0.7.

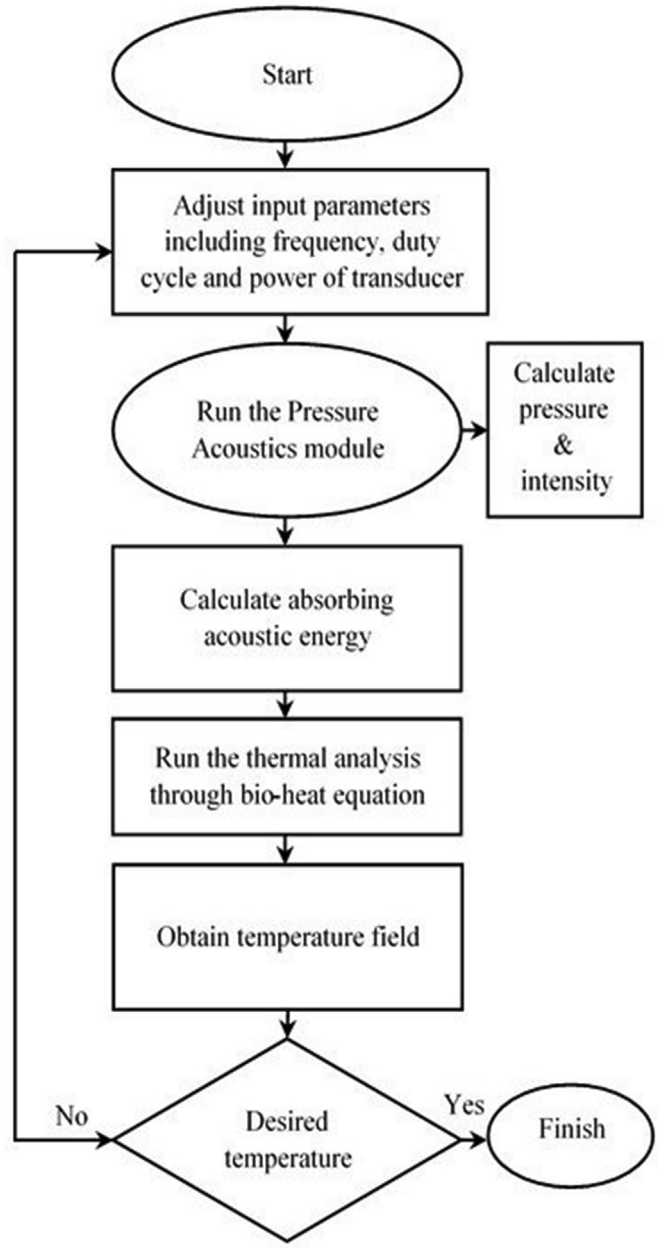

Fig. 6. Flowchart of the computational algorithm.

2.6. Artificial neural networks

Artificial neural networks are computing methods which are used in machine learning and knowledge representation in order to prognosticate output response of complicated systems. This system consists of a large number of super-integrated processing elements called neurons that work together to solve a problem and transmit information through synapses (electromagnetic communications).

In this study, a two-layer feedforward neural network (*FFNN*) is used to provide the correlation between the transducer operating parameters and the desired temperature rise. In the subsequent inverse analysis, maximum temperature rise is the input of the network to obtain required values of frequency, normal displacement and duty cycle. According to Table 5, a total number of 30 analyses are conducted which are divided into 24 training and 6 testing datasets.

In machine learning sometimes despite good training performance, the testing performance can be completely different and the network cannot perform as a good prediction model. In *K*-fold cross-validation, the input data is randomly divided into *K* equal-sized groups which one of these groups is maintained for validation and testing of the model, while the other groups are feed to the network as training data. Thus, it is desired to employ *K*-fold cross-validation for stabilizing the performance of the proposed network. In the present study, 5-fold cross-validation is utilized in which the data is repositioned to make sure that each fold is a good show of the whole dataset. In this regard, 30 datasets are randomly divided into 5 groups consisting of 6 trials in each group. The values of *RMSE* for the five models are calculated to be 0.2012, 0.1028, 0.1101, 0.0882 and 0.0931 and the mean value of *RMSE* is 0.1190. Small values of *RMSE* imply that the accuracy of the model is acceptable and the proposed neural network is independent of the selection of datasets.

The transducer operating parameters are employed as the inputs of the network while the maximum temperature in the tumoral region is the output. Details of the *FFNN* properties are listed in Table 6.

Two statistical parameters including the efficiency (*E*) and the root mean squared error (*RMSE*) (Eq. (8) and Eq. (9)) are used to assess the performance of the network.

$$RMSE = \sqrt{\left[\sum_{i=1}^{N} \frac{(X_d - X_s)^2}{N}\right]} \tag{8}$$

$$E = \frac{\sum_{i=1}^{N} (X_d - \bar{X}_s)^2 - \sum_{i=1}^{N} (X_d - X_s)^2}{\sum_{i=1}^{N} (X_d - \bar{X}_s)^2} \tag{9}$$

where X_d, X_s, $\bar{X}_d$, $\bar{X}_s$ are the desired variables, estimated variables, average of the desired variables and the average of estimated variables, respectively.

3. Results

3.1. Validation and nonlinear effects

The *FUS* simulation is validated by employing the *HIFU* simulator for the *2DNT* model. Fig. 7a and b shows the absolute pressure variation along a path passes from the focal point in z-direction (path A-B in Fig. 1a) for the frequency of 1 and 3 MHz and normal displacement of 1 and 5 nm. According to this figure, relative difference between the results is less than 8% at the frequency of 3 MHz, which proves the reliability of *FUS* simulation in the present study. Subsequently, *HIFU* simulator results are used to study the significance of nonlinear effect in the aforementioned operating conditions. Fig. 7c and d compare the absolute pressure variation obtained from the *HIFU* simulator with the *2D* brain model without considering the vascular network. The acoustic pressure is obtained on path C-D which has been displayed in Fig. 1b. It

Table 5
Input values for each calculation.

Model	*2DVT*						*3DST*
Frequency	1 MHz			3 MHz			1 MHz
Duty cycle	0.7	0.8	1	0.7	0.8	1	1
Normal displacement value	1–5 nm	1–5 nm	1–5 nm	1–5 nm	1–5 nm	1–5 nm	1–5 nm

Table 6
Artificial neural network's properties.

Training function	Performance function	Number of inputs	Number of outputs	Transfer function	Number of neurons in 1st layer	Number of neurons in 2nd layer	Number of epochs
Trainbr	MSE	3	1	Tansig	3	1	10000

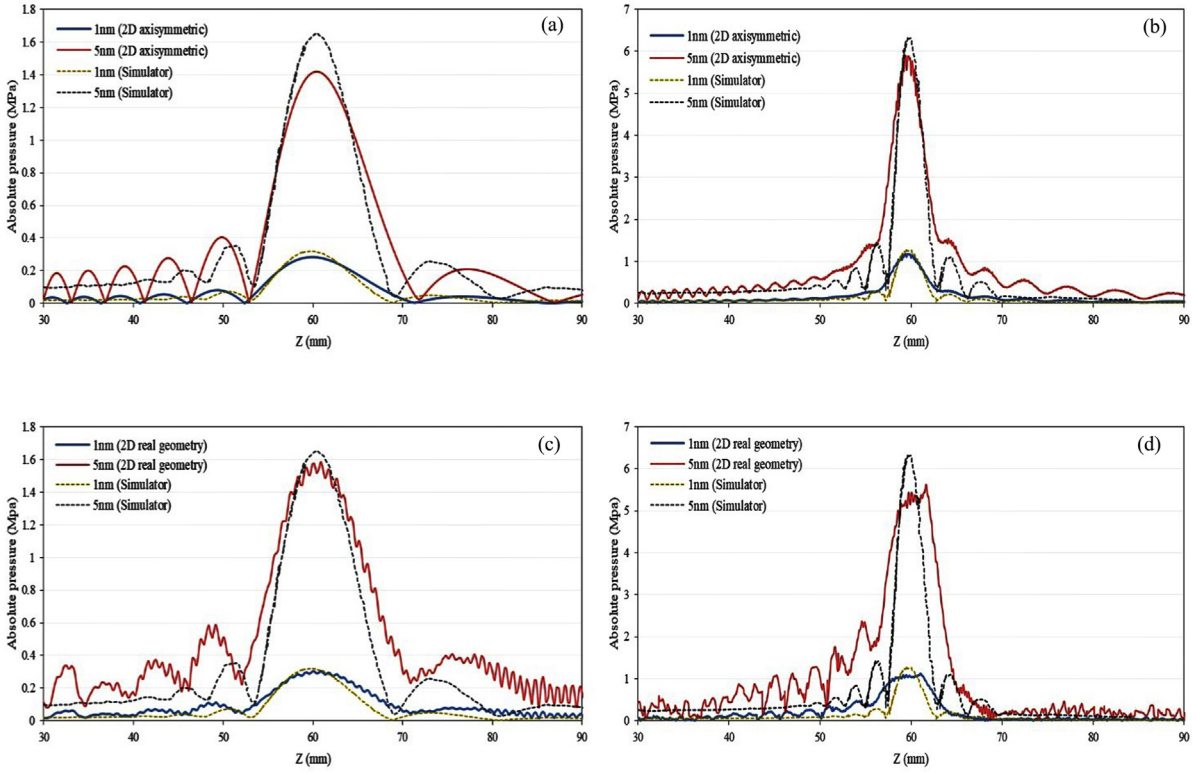

Fig. 7. Comparison of absolute pressure on a path in z-direction passes from the focal point obtained by HIFU simulator and (a) *2DNT* results at frequency of 1 MHz, (b) *2DNT* results at frequency of 3 MHz, (c) *2D* real model results at frequency of 1 MHz, (d) *2D* real model results at frequency of 3 MHz.

is concluded that the maximum absolute pressure by considering the nonlinear effect increases by 5% at the frequency of 1 MHz and by 12% at the frequency of 3 MHz.

Insignificant nonlinearity effect is the main reason for using low powers of the transducer in the present study. Meanwhile, it has been demonstrated that low transducer power is adequate to provide irreversible ablation of the tumor (Bini et al., 2018) where low acoustic power is used for qualitative description of 5W. This is due to the role of the exposure time in addition to the transducer power. Moreover, at low transducer powers, the temperature increase in the targeted tissue in clinical applications could be better controlled. This would bring more comfort for the patient during *FU* treatment (Bini et al., 2018; Kotewall and Lang, 2019).

However, to carry out the nonlinear *2D* simulation of brain tissue, up to 170 h calculation is required on a computing system with 32 cores and 42 GB RAM. To avoid excessive computational time due to high transducer powers, low powers are employed and nonlinear modeling is therefore unnecessary.

3.2. Pressure-temperature profile for model 2DVT

The acoustic pressure distribution is obtained in the healthy and tumoral tissues in the steady state according to Eqs. (1)–(3). Surface plot of the acoustic pressure field in the brain and in the tumor are illustrated in Fig. 8. Fig. 8a and b displays the acoustic pressure contours for normal displacement of 1 nm and 2 nm applied by the transducer to the brain surface, respectively. According to Eq. (4), doubling the normal displacement corresponds to 4-fold increase of the wave intensity and the ultrasound power.

With regard to this figure, pressure extrema appear in the tumoral domain. By doubling the normal displacement, the extremum pressures increase by 5 times and the pressure profile becomes steeper around the local extrema.

Maximum and minimum pressures are extracted for normal displacements of 1 nm, 2 nm, 3 nm, 4 nm, and 5 nm and are presented in Table 7. To provide the inputs of an inverse analysis for obtaining the transducer operating parameters for the desired temperature rise, effect of frequency variation on the acoustic pressure is considered alongside the wave intensity. It is observed that maximum positive and minimum negative pressures occur for the frequency of 3 MHz and normal displacement amplitude of 5 nm. The trend of pressure variation implies that increasing frequency and normal displacement amplitude of the transducer results in the elevation of maximum and minimum acoustic pressures in the tumor.

In order to acquire temperature distribution, the amount of absorbed ultrasound energy is obtained by Eq. (5) and is employed as the heat source in Pennes bio-heat transfer equation. By identifying the temperature profile in the tissue, the thermal dose function could be identified. Exposure time is 10s considering constant and pulse ultrasound waves. The temperature profiles are presented in Fig. 9 for two frequencies of 1 MHz and 3 MHz and the normal displacement of 3 nm. With regard to these figures, the extrema of pressure in the tumoral

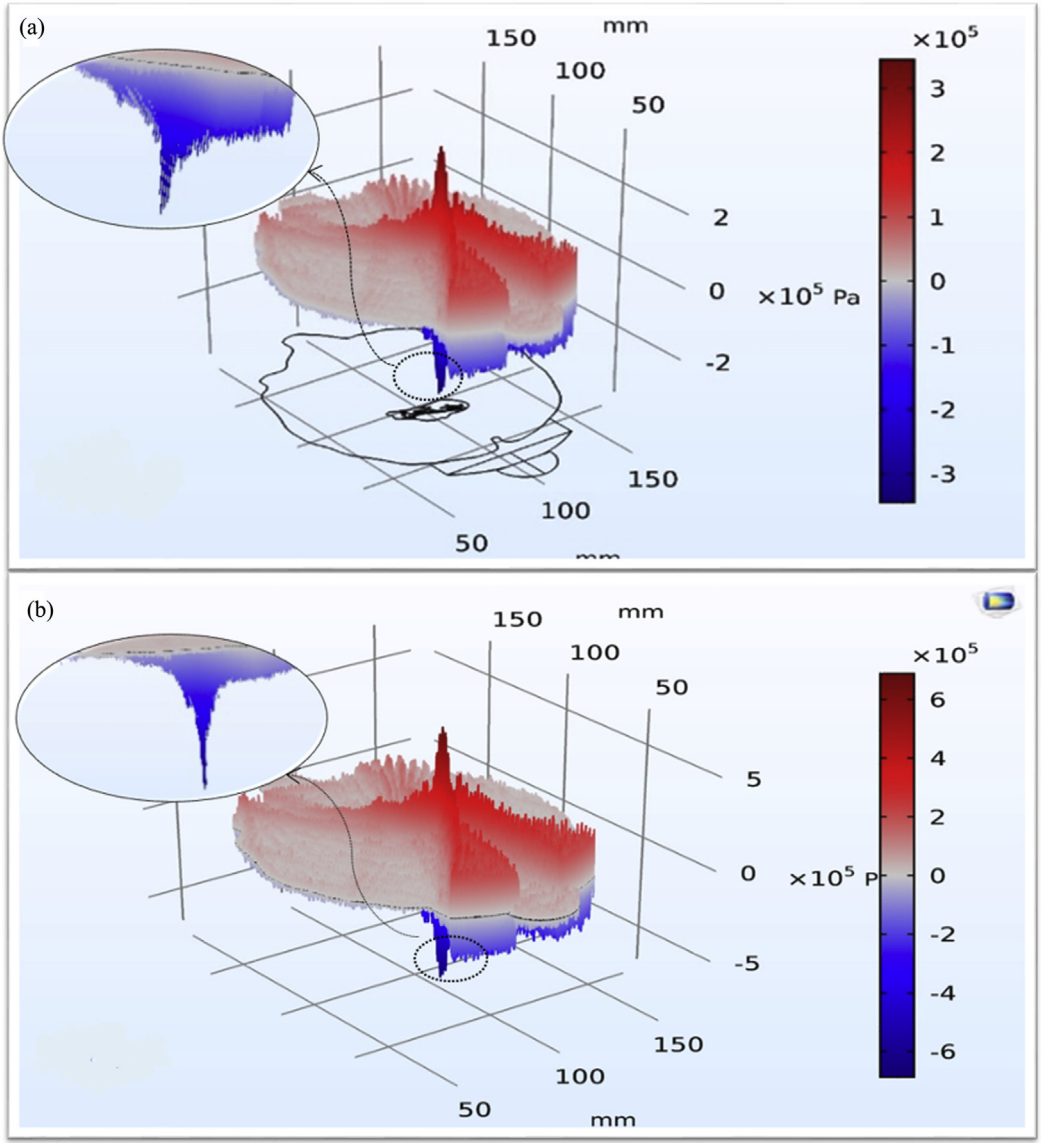

Fig. 8. Linear acoustic pressure distribution throughout the brain tissue exposed for 10s to the ultrasound beam with normal displacement of (a) 1 nm, (b) 2 nm.

Table 7
Peak positive and negative pressures throughout the brain tissue for different normal displacements and transducer frequencies.

Frequency	1 MHz					3 MHz				
Normal displacement amplitude (nm)	1	2	3	4	5	1	2	3	4	5
Maximum pressure (MPa)	0.344	0.689	1.033	1.378	1.723	1.730	3.461	5.192	6.923	8.654
Minimum pressure (MPa)	−0.343	−0.687	−1.032	−1.375	−1.719	−1.761	−3.522	−5.284	−7.045	−8.806

region act as source of energies which result in the appearance of two maxima in the temperature profile according to Eq. (5). Moreover, it can be observed that the ultrasound beam with higher frequency is focused to a more limited area in the tumoral tissue while the wave intensity and resultant temperature rise are significantly increased in the focal area. For the frequencies of 1 MHz, 5 K temperature rise is observed in the focal area. This value reaches to 60 K for the frequency of 3 MHz.

Thermal damage to adjacent healthy tissue could be minimized by using pulse wave with a specified duty cycle. The effect of different duty cycles on temperature profile is studied in the tumoral tissue. Afterward, temperature variation is studied in the healthy tissue through the thermal dose function. To obtain the correlation between duty cycle and temperature profile, a reference point (*R.P.*) is defined near the blood vessels in the tumoral region in the focal area. At this point, the temperature rise is studied during 10s of exposure time.

The temperature rise of *R.P.* is extracted during the exposure time for different duty cycles and two frequencies of 1 MHz and 3 MHz and normal displacement of 3 nm in Table 8. For different duty cycles, the temperature rise differs during the off periods. In these periods, values of temperature rise for constant wave are higher than the pulse wave. This is due to the lack of propagation of ultrasound waves inside the brain tissue during these time periods.

Temperature distribution inside the tumoral tissue is a crucial factor that determines the volume of damaged tissue. The area of maximum and minimum temperature rise should be known in order to

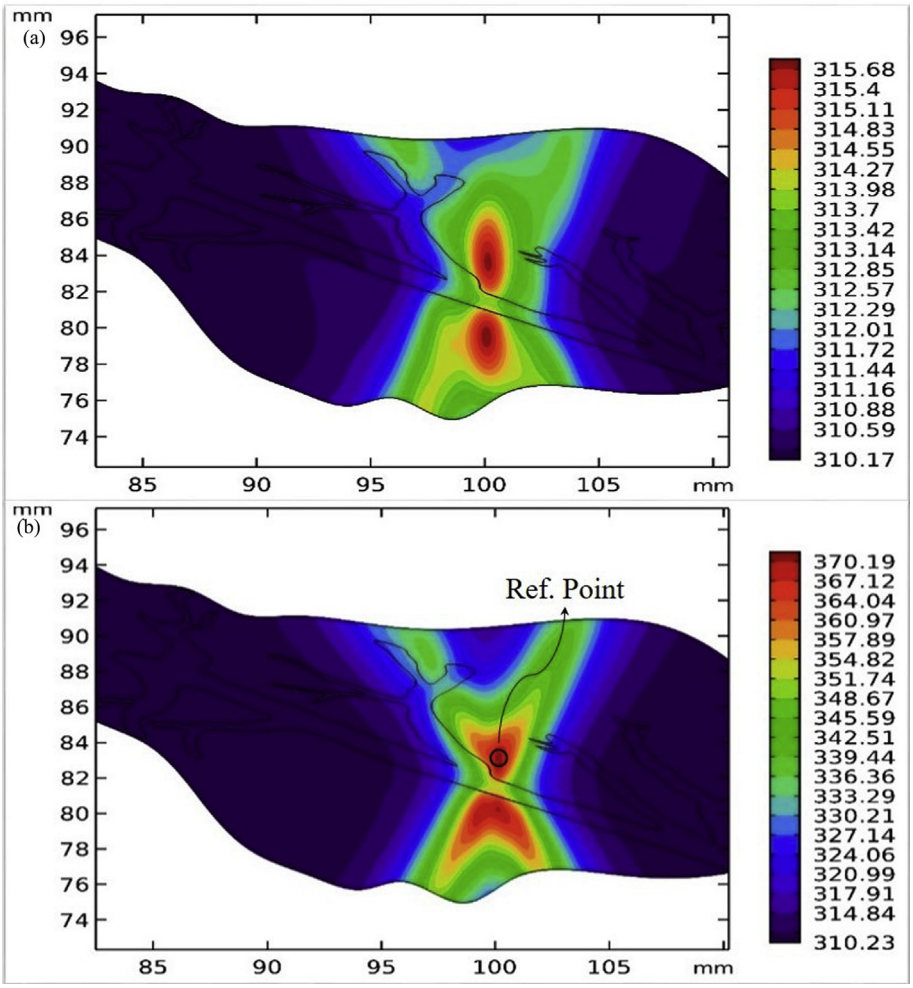

Fig. 9. Isothermal contours in the tumoral tissue and blood vessels for normal displacement of 3 nm and frequency of (a) 1 MHz (b) 3 MHz; a reference point is indicated near the blood vessels for temperature measurement.

Table 8
Temperature rise of *R.P.* with normal displacement of 3 nm during the exposure time for different duty cycles.

Frequency		1 MHz			3 MHz		
Duty cycle		0.7	0.8	1	0.7	0.8	1
Temperature increase	at 2s	1.7381	1.8223	1.8224	18.9751	20.1450	20.1451
	at 4s	2.8482	2.9058	2.9059	31.5756	32.6268	32.6270
	at 6s	3.7611	3.7999	3.8000	42.0801	42.7315	42.7321
	at 8s	4.5797	4.6075	4.6080	51.3560	51.7925	51.7932
	at 10s	5.3356	5.3564	5.3570	59.7835	60.1039	60.1040

prognosticate the most affected area. Fig. 10 demonstrates location of maximum and minimum temperature rises in the tumor and in the blood vessels. While the focal area has significant temperature increase, the adjacent tissues have insignificant temperature rise and almost have normal body temperature.

To provide inputs of the inverse analysis, maximum and minimum temperature rises are extracted from thermal analysis for different normal displacements and frequencies inside the tumor and the blood vessels. Values of maximum and minimum temperature rise are listed in Table 9.

Results show that the values of temperature elevation inside the tumoral tissue are higher than the blood vessels. In comparison to tumoral tissue, the amount of absorbed acoustic energy by the blood vessels is small. Generally, this phenomenon is known as blood cooling effect which leads to a smaller temperature rise inside the blood domain.

3.3. Pressure-temperature profile for model 3DST

Homogeneous Helmholtz and bio-heat transfer equations have also been solved for *3D* real geometry of brain tissue. Three-dimensional simulation is greatly restricted by the computational costs. Different powers of transducer are applied to the *3D* model with the frequency of 1 MHz. Table 10 lists the values of peak positive and negative pressures which occur inside the tumor.

To acquire distribution of temperature elevation inside the tumoral tissue, a reference point is defined inside the focal area. Fig. 11a shows where this point is located and plot of the temperature increase at this point during 10s of exposure time is demonstrated in Fig. 11b. Considering the pressure as a heat source, extrema of temperature occur in the tumor. Increase of the temperature gradient with the transducer power is observed.

Considering the fact that the geometry of blood vessels is not considered in the *3D* simulation, there is a source of uncertainty in the obtained results. In the work done by Solovchuk et al., (2013) the maximum temperature increase within the focal area was 41.8 °C in the absence of blood flow, while this value was 38.8 °C for the parallel flow. In another study carried out by Solovchunk et al. (Solovchuk et al., 2015) with the sonication time of 0.4s, the difference between maximum temperature within tumoral tissue and portal vein was approximately 4 °C. In the present study, the maximum temperature difference

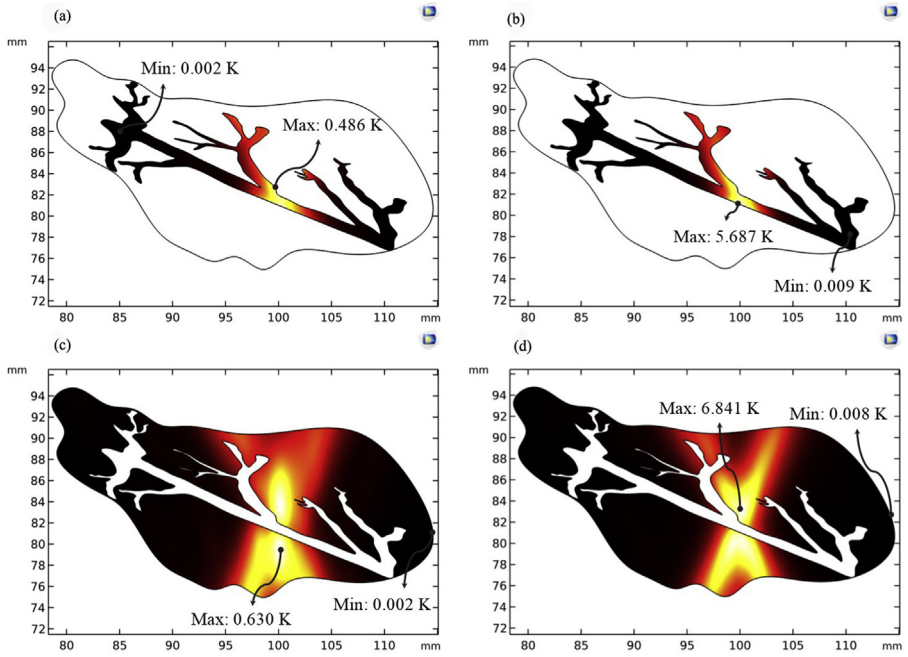

Fig. 10. Location of maximum and minimum temperatures for the frequencies of 1 MHz and 3 MHz with normal displacement of 1 nm, (a) inside blood vessels with frequency of 1 MHz, (b) inside blood vessels with frequency of 3 MHz, (c) inside tumor with frequency of 1 MHz, (d) inside tumor with frequency of 3 MHz.

Table 9
Maximum and minimum temperature rises inside blood vessels and tumoral tissue.

Normal displacement amplitude		1 MHz		3 MHz	
		Maximum temperature increase (K)	Minimum temperature increase (K)	Maximum temperature increase (K)	Minimum temperature increase (K)
Blood vessels	1 nm	0.4863	0.0023	5.6874	0.0088
	2 nm	1.9454	0.0092	22.750	0.0352
	3 nm	4.3771	0.0207	51.190	0.0793
	4 nm	7.7815	0.0368	91.009	0.1410
	5 nm	12.159	0.0575	142.21	0.2203
Tumoral tissue	1 nm	0.6300	0.0022	6.8412	0.0083
	2 nm	2.5202	0.0090	27.3660	0.0335
	3 nm	5.6705	0.0202	61.578	0.0754
	4 nm	10.0810	0.0360	109.48	0.1340
	5 nm	15.751	0.0563	171.08	0.2094

Table 10
Maximum and minimum acoustic pressures inside the tumor for different normal displacements.

Frequency	1 MHz				
Normal displacement amplitude (nm)	1	2	3	4	5
Maximum pressure (MPa)	1.005	2.010	3.015	4.020	5.025
Minimum pressure (MPa)	−1.103	−2.207	−3.310	−4.414	−5.517

between domains of tumoral tissue and blood vessels for the normal displacement of 3, 4 and 5 nm in *2D* simulation is 1.3, 2.3 and 3.6 °C, respectively. These results provide some information regarding the error associated with the omission of the blood cooling effect near large blood vessels in *3D* simulation.

Wave intensity profile and the resultant temperature increase profile as a result of 1 nm normal displacement, frequency of 1 MHz and constant ultrasound wave are provided in Fig. 12 after 10s of exposure time and for a section of brain tissue. With the beam intensity concentrated in the focal area, the profile of temperature increase is more localized.

Maximum and minimum intensity magnitudes in the focal area for different transducer powers and for the frequency of 1 MHz are listed in Table 11.

3.4. Calculation of thermal dose function

In order to obtain optimum treatment which corresponds to maximum tumor ablation and minimum healthy tissue trauma, the thermal dose function is obtained for two-dimensional (*2DVT*) and three-dimensional (*3DST*) models by using Eq. (7). Fig. 13a and b demonstrate the values of thermal dose function in *2D* model of brain tissue for the frequencies of 1 MHz and 3 MHz after 10s exposure to the ultrasound beam. Maximum thermal dose is 1000 times more for the frequency of 3 MHz compared to 1 MHz in the focal area. It is worth to notice that the affected area in the healthy region is insignificant for the frequency of 3 MHz compared to 1 MHz and the distribution of thermal dose is much more localized to the tumoral tissue. Fig. 13c presents the thermal dose distribution for the *3D* model for the frequency of 3 MHz and exposure time of 10s. A comparison between results of Figs. 13a and c implies that the thermal dose is one order of magnitude smaller in the *2D* model which is mainly due to the blood cooling effect of the vascular network.

For better comparison among different normal displacement and frequency values, maximum and minimum values of thermal dose are listed in Table 12.

3.5. Artificial neural network analysis

For two-dimensional real geometry of brain tissue with vascular tumor (*2DVT* model), the *FFNN* is trained. Fig. 14a displays values of estimated temperature obtained by the network and their corresponding values calculated by numerical modeling for the whole datasets including training and testing datasets. Moreover, regression analysis over the whole datasets is provided in Fig. 14b. It is observed that the estimated values of the maximum temperature are very close to the real values. The regression coefficient is very close to 1.

E-values equal to 1, and *RMSE*-values equal to zero are indicative of

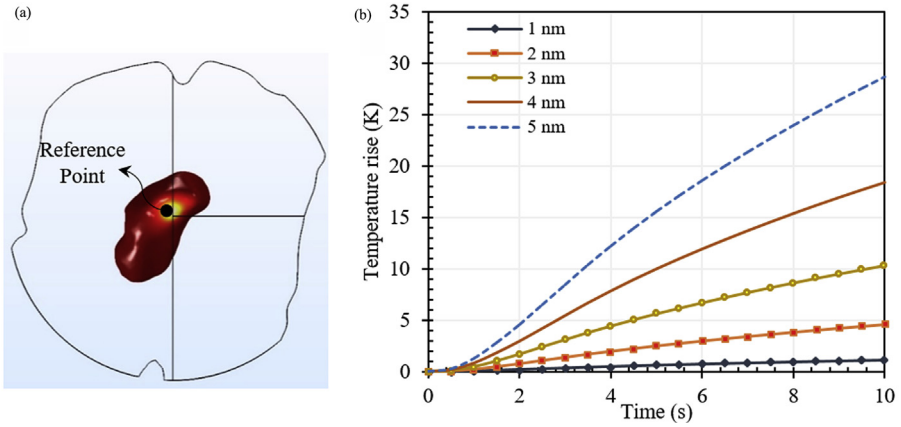

Fig. 11. (a) Location of the reference point for temperature measurement, (b) plots of temperature increase for different values of normal displacement and with the frequency of 1 MHz.

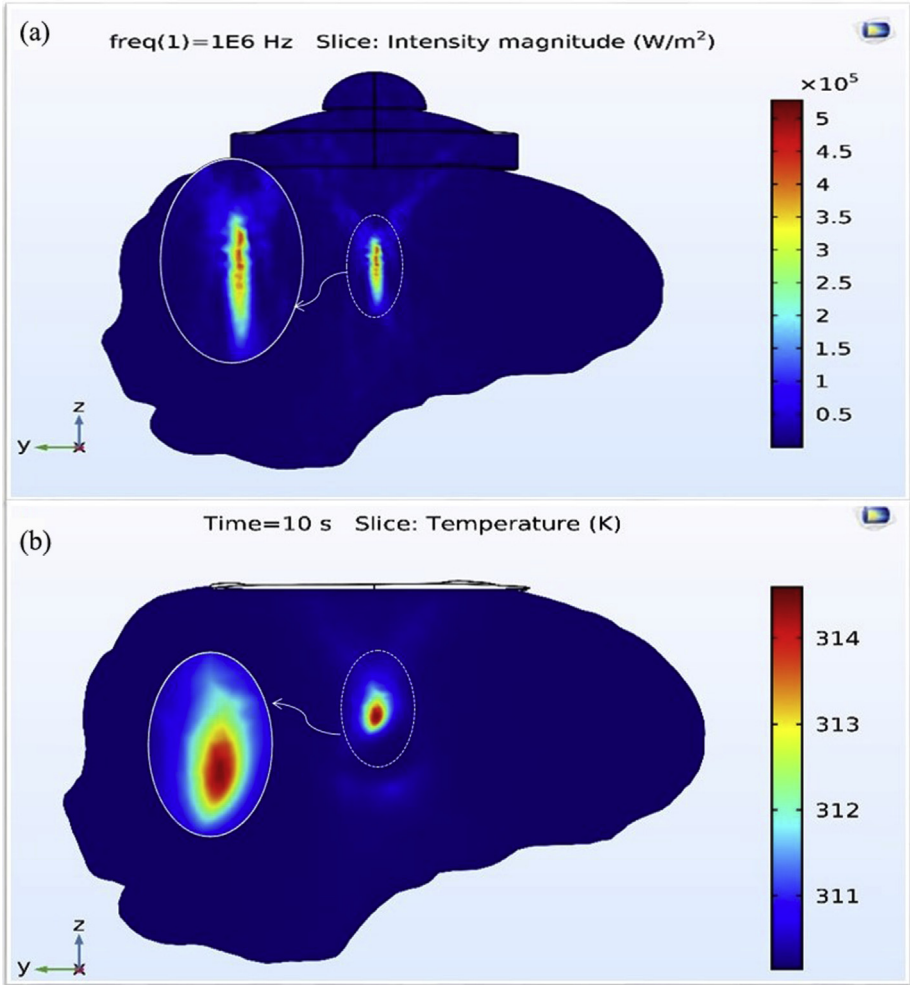

Fig. 12. (a) Contours of intensity magnitude, (b) contours of temperature increase, for normal displacement of 1 nm, and frequency of 1 MHz after 10s of exposure time.

the perfect performance of the network. *E* and *RMSE* values for training datasets are 1 and 0.0288, respectively, which imply high performance of the proposed network in estimating the maximum temperature in the focal area located in the tumoral region versus the transducer's operating parameters.

4. Discussion

Numerical simulation demonstrates that by changing the operating parameters of the focused ultrasound transducer, i.e. the frequency, duty cycle and the power, the required temperature distribution for optimum *FUS* can be obtained. For optimum treatment, the temperature rise of tumoral tissue should be high to attain irreversible tissue

Table 11
Maximum and minimum intensities in the focal area for different normal displacements.

Frequency	1 MHz				
Normal displacement amplitude (nm)	1	2	3	4	5
Maximum intensity $\left(\frac{W}{m^2}\right)$	3.85E5	1.54E6	3.47E6	6.17E6	9.64E6
Minimum intensity $\left(\frac{W}{m^2}\right)$	7.24	28.98	65.217	115.94	181.16

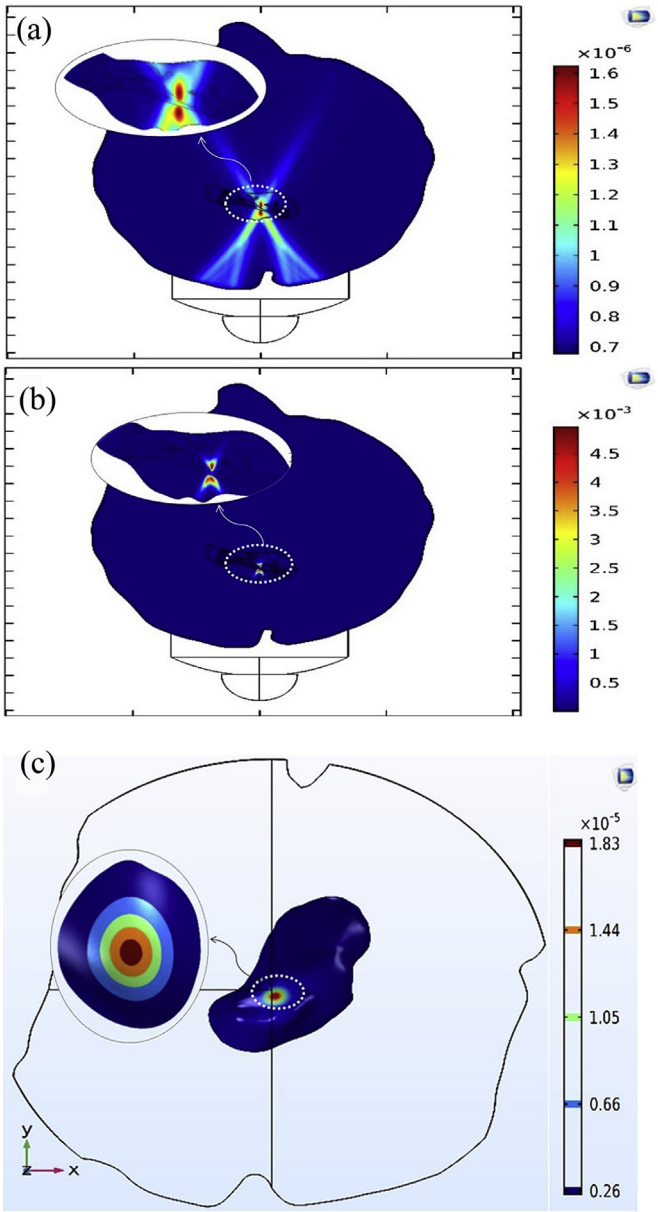

Fig. 13. Thermal dose contours for (a) *2DVT* model at frequency of 1 MHz, (b) *2DVT* model at frequency of 3 MHz, and (c) *3DST* model at frequency 1 MHz, while normal displacement is 1 nm and exposure time is 10s, the affected area is magnified.

damage and the temperature rise of the healthy tissue should be relatively small to avoid undesirable damage.

Acoustic pressure field for model *2DVT* reveals that peak positive and negative pressures occur in the tumoral region. Phenomena such as cavitation and acoustic streaming may also have effects on the induced pressure. Cavitation phenomenon is an important effect which has not been considered in this study. It has been proven that cavitation formation can accelerate the rate of tumor destruction. Moreover, increase of the pressure value causes an ultrasound-induced heating which acts as a heat source. Thus, the resultant temperature rise profile strongly depends on the frequency and power of the transducer.

The computed temperature profiles reveal that the shape of damaged area is significantly different for the frequencies of 1 MHz and 3 MHz. The reason is that there are different amount of penetration rates for each frequency. At lower frequency the temperature rise is smaller and the affected area is larger compared to the higher frequency. With regard to this fact, lower frequency is usually used in physiotherapy where the temperature rise does not cause irreversible damages to the tissue. Higher frequency has application in tumor ablation where high temperature causes cell necrosis confined to the tumoral region.

If the values of thermal dose surpass a specified threshold, the target tissue is going to be damaged. Based on existing studies (Canney et al., 2008; Dewey, 2009), the thermal dose threshold for cell death is in the range of $100\text{min} < TD_{43} < 1000\text{min}$. Assessing the thermal dose acquired in the present study shows that some of the trials belong to this bound.

In order to control the damaged area, pulsatile ultrasound waves are preferred. Results imply that in case of constant wave, higher temperature rise is obtained. However, for reducing damage to adjacent tissue, pulse wave should be employed during the treatment.

Presence of the blood vessels provides the cooling effect in the tumoral tissue. Absorption of the sound wave energy in the tumoral tissue becomes less in the presence of blood vessels in tumor. Meanwhile, the blood vessels absorb less energy than the tissue. The difference between maximum temperature in the blood vessels and the tumoral tissue is 23% and 16% for the frequencies of 1 MHz and 3 MHz, respectively. This issue should be considered for tumor ablation in the vascular phase. In this phase, cooling effect is significant and in order to acquire the desired temperature in the tumor, employment of more power and intensity is suggested.

Results of several simulations for the *2DVT* are used to train an artificial neural network. Evaluation of the network shows its applicability and reliability in estimating the transducer parameters to acquire the desired temperature. However, it is worth noticing that in practical medical use, the transducer parameters cannot be easily set to the obtained values by the network and one should select the closest values according to the ultrasonic device specifications. Moreover, the network has the capability of fixing some input parameters and specifying the remaining parameters to achieve the desired output.

Numerical modeling of *3DST* for the frequency of 1 MHz demonstrates that the two-dimensional simulation has indispensable differences with the three-dimensional modeling. Due to neglecting the microvessels in the *3D* simulation, pressure-temperature values have noticeable elevation compared to the *2D* results. However, the pattern of temperature variation with the transducer operating parameters is similar to the *2D* results.

In the present study, the maximum focal intensity for model *3DST* is $964\frac{w}{cm^2}$. Surprisingly, new *HIFU* devices generate high focal intensities varying from a few thousands of $\frac{w}{cm^2}$ to more than 25,000 $\frac{w}{cm^2}$ and can focus the ultrasound power to a small-sized focal spot.

5. Conclusions

In the present study, the size of thermal lesion induced by *FU* is optimized through hyperthermia treatment of brain malignant tumor during intraoperative brain surgery. In order to investigate effects of focused acoustic waves in the focal area, two-dimensional geometry of brain tissue with a malignant vascular tumor is modeled based on *MRI* images. For the *FUS* simulation, an ultrasound transducer is used to

Table 12
Maximum and minimum values of thermal dose inside the focal area.

Geometry	*3DST* (1 MHz)				*2DVT* (1 MHz)					*2DVT* (3 MHz)		
Normal displacement (nm)	1	2	3	4	1	2	3	4	5	1	2	3
Maximum thermal dose	2.0E-5	3.8E-2	186.7	2.5E7	1.6E-6	2.2E-5	1.7E-3	4.7E-2	2.3	4.9E-3	7507.8	1.4E14
Minimum thermal dose	6.8E-7	7.1E-7	7.6E-7	8.3E-7	6.8E-7	6.8E-7	6.9E-7	7.1E-7	7.3E-7	6.8E-7	7.1E-7	7.5E-7

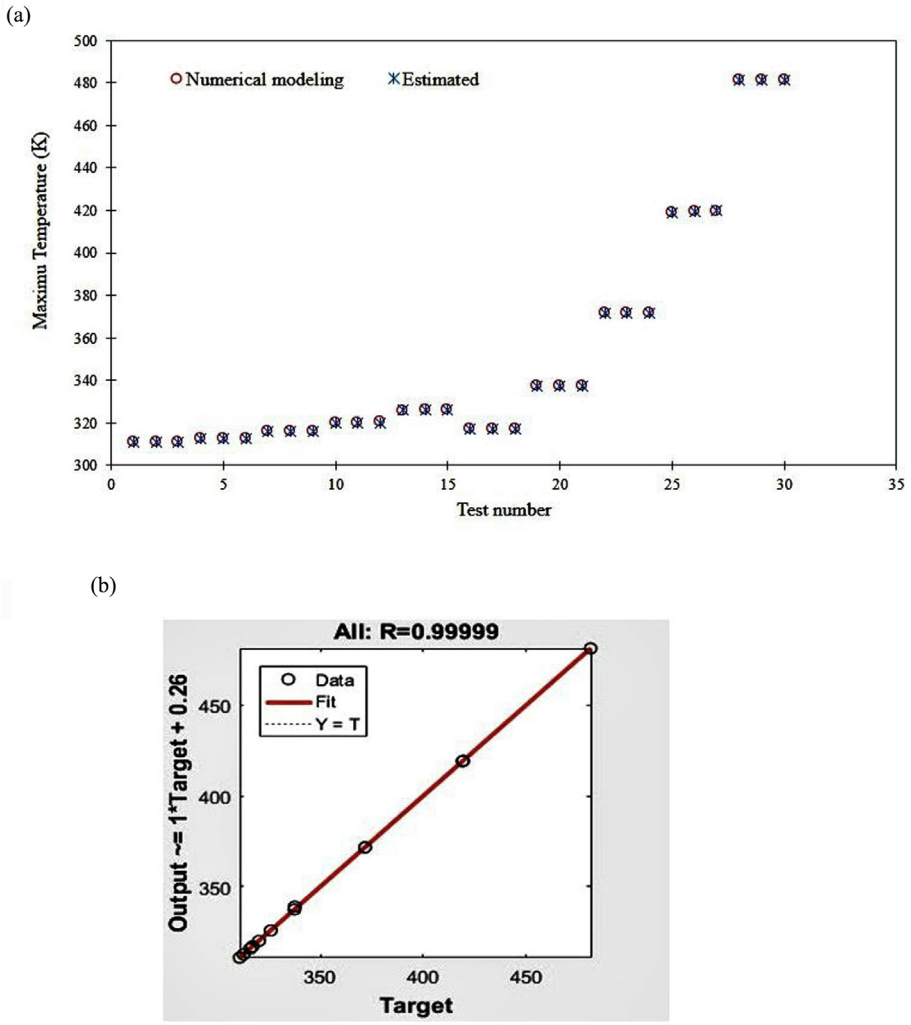

Fig. 14. (a) Maximum temperature obtained from the numerical modeling and the *FFNN*, (b) regression analysis, for the whole datasets.

generate focused beams which induce significant pressure and temperature variations in the focal zone. For calculation of acoustic wave propagation, homogeneous Helmholtz equation is used and pressure profile is obtained. The pressure acts as the source of extra heat generation in the brain tissue for thermal analysis through the bio-heat transfer equation. Temperature profile in the brain tissue is utilized as an input for calculation of thermal dose function which indicates the profile of irreversible damage to the tissue. Moreover, maximum temperature rise is used as the output of an artificial neural network to estimate the transducer operating parameters including the power, and the frequency and duty cycle of the pulse wave.

Results show that the temperature profile has strong correlation with the transducer operating parameters. By increasing the frequency, normal displacement, and duty cycle of the pulse wave, the temperature rise increases in the focal area which is located in the tumoral region. Moreover, by increasing the frequency, the temperature rise is more concentrated around the focal point. A feedforward artificial neural network is used to obtain the desired temperature rise by adjusting the transducer parameters. Analysis of the network through the calculation of efficiency and *RMSE* indicates high performance of the network.

To make the simulation more realistic, a three-dimensional model is considered by neglecting the blood vessels in the tumoral tissue. Higher temperature rise relative to the *2D* model indicates the importance of considering blood cooling effect in the vascular tumor.

To assess the performance of *FUS* in thermal ablation of brain tumor, thermal dose function is calculated in the *2D* and the *3D* models. Results of the thermal dose function indicate that some of the trials surpass the threshold which is required for cell death in the tumoral tissue. However, in these examples the healthy brain tissue does not experience any irreversible damage.

Altogether, it can be stated that for acquiring desired thermal lesion, ultrasound waves should be used in the form of pulse waves with different time periods. Also, due to presence of microvessels, the cooling effect should be considered in order to obtain desired thermal treatment.

Funding

This research did not receive any specific grant from funding agencies in the public, commercial, or not-for-profit sectors.

Conflict of interest

The authors declare that they have no conflict of interest.

Ethical approval

All procedures followed were in accordance with the ethical standards of the responsible committee on human experimentation (institutional and national) and with the Helsinki Declaration of 1975, as revised in 2000 (5). Informed consent was obtained from all patients for being included in the study.

Appendix A. Supplementary data

Supplementary data to this article can be found online at https://doi.org/10.1016/j.jtherbio.2019.05.019.

References

Almekkaway, M.K., Shehata, I.A., Haritonova, A., Ballard, J., Casper, A., Ebbini, E., 2017. Image-based numerical modeling of HIFU-induced lesions. In: AIP Conf Proc AIP Publishing, pp. 20001.

Amini, S.M., 2018. Gold nanostructures absorption capacities of various energy forms for thermal therapy applications. J. Therm. Biol. Elsevier 79, 81–84.

Beik, J., Abed, Z., Ghadimi-Daresajini, A., Nourbakhsh, M., Shakeri-Zadeh, A., Ghasemi, M.S., Shiran, M.B., 2016. Measurements of nanoparticle-enhanced heating from 1 MHz ultrasound in solution and in mice bearing CT26 colon tumors. J. Therm. Biol. Elsevier 62, 84–89.

Billard, B.E., Hynynen, K., Roemer, R.B., 1990. Effects of physical parameters on high temperature ultrasound hyperthermia. Ultrasound Med. Biol. Elsevier 16, 409–420.

Bini, F., Trimboli, P., Marinozzi, F., Giovanella, L., 2018. Treatment of benign thyroid nodules by high intensity focused ultrasound (HIFU) at different acoustic powers: a study on in-silico phantom. Endocr. Springer 59, 506–509.

Canney, M.S., Bailey, M.R., Crum, L.A., Khokhlova, V.A., Sapozhnikov, O.A., 2008. Acoustic characterization of high intensity focused ultrasound fields: a combined measurement and modeling approach. J. Acoust. Soc. Am. ASA 124, 2406–2420.

De Greef, M., Kok, H.P., Correia, D., Bel, A., Crezee, J., 2010. Optimization in hyperthermia treatment planning: the impact of tissue perfusion uncertainty. Med. Phys. Wiley Online Libr. 37, 4540–4550.

Dewey, W.C., 2009. Arrhenius relationships from the molecule and cell to the clinic. Int. J. Hyperth. Taylor Francis 25, 3–20.

Dromi, S., Frenkel, V., Luk, A., Traughber, B., Angstadt, M., Bur, M., Poff, J., Xie, J., Libutti, S.K., Li, K.C.P., 2007. Pulsed-high intensity focused ultrasound and low temperature–sensitive liposomes for enhanced targeted drug delivery and antitumor effect. Clin. Canc. Res. AACR 13, 2722–2727.

Duck, F.A., 1990. Electrical properties of tissue. Phys. Prop. Tissue Acad. 167–223.

Escoffre, J.-M., Bouakaz, A., 2015. Therapeutic Ultrasound. Springer.

Folkman, J., 1990. What is the evidence that tumors are angiogenesis dependent? JNCI J. Natl. Cancer Inst. Citeseer 82, 4–7.

Galleries, K.I.P., 2013. Blood Vessels in a Glioblastoma. Available from: https://ki-galleries.mit.edu/2013/blauvelt.

Gholami, M., Haghparast, A., Dehlaghi, V., 2017. Numerical study for optimizing parameters of high-intensity focused ultrasound-induced thermal field during liver tumor ablation: HIFU Simulator. Iran J. Med. Phys. 14, 15–22.

Guan, L., Xu, G., 2016. Damage effect of high-intensity focused ultrasound on breast cancer tissues and their vascularities. World J. Surg. Oncol. BioMed. Central 14, 153.

Guntur, S.R., Choi, M.J., 2015. Influence of temperature-dependent thermal parameters on temperature elevation of tissue exposed to high-intensity focused ultrasound: numerical simulation. Ultrasound Med. Biol. Elsevier 41, 806–813.

Hariharan, P., Myers, M.R., Banerjee, R.K., 2007. HIFU procedures at moderate intensities—effect of large blood vessels. Phys. Med. Biol. IOP Publ. 52, 3493.

Huang, J., Holt, R.G., Cleveland, R.O., Roy, R.A., 2004. Experimental validation of a tractable numerical model for focused ultrasound heating in flow-through tissue phantoms. J. Acoust. Soc. Am. ASA 116, 2451–2458.

Huang, H.-W., Shih, T.-C., Liauh, C.-T., 2010. Predicting effects of blood flow rate and size of vessels in a vasculature on hyperthermia treatments using computer simulation. Biomed. Eng. Online BioMed. Central 9, 18.

Huang, C.W., Sun, M.K., Chen, B.T., Shieh, J., Chen, C.S., Chen, W.S., 2015. Simulation of thermal ablation by high-intensity focused ultrasound with temperature-dependent properties. Ultrason. Sonochem. Elsevier 27, 456–465.

Kok, H.P., Van den Berg, C.A.T., Bel, A., Crezee, J., 2013. Fast thermal simulations and temperature optimization for hyperthermia treatment planning, including realistic 3D vessel networks. Med. Phys. Wiley Online Libr. 40.

Kok, H.P., Kotte, A., Crezee, J., 2017. Planning, optimisation and evaluation of hyperthermia treatments. Int. J. Hyperth. Taylor Francis 33, 593–607.

Kotewall, N., Lang, B.H.H., 2019. High-intensity focused ultrasound ablation as a treatment for benign thyroid diseases: the present and future. Ultrasonogr. Korean Soc. Ultrasound. Med. 38, 135.

Mascheroni, P., Stigliano, C., Carfagna, M., Boso, D.P., Preziosi, L., Decuzzi, P., Schrefler, B.A., 2016. Predicting the growth of glioblastoma multiforme spheroids using a multiphase porous media model. Biomech. Model. Mechanobiol. Springer 15, 1215–1228.

Okita, K., Ono, K., Takagi, S., Matsumoto, Y., 2010. Numerical simulation of the tissue ablation in high-intensity focused ultrasound therapy with array transducer. Int. J. Numer. Methods Fluid. Wiley Online Libr. 64, 1395–1411.

Peek, M.C.L., Ahmed, M., Douek, M., 2015. High-intensity focused ultrasound for the treatment of fibroadenomata (HIFU-F) study. J. Ther. Ultrasound BioMed. Central 3, 6.

Pennes, H.H., 1998. Analysis of tissue and arterial blood temperatures in the resting human forearm. J. Appl. Physiol. Am. Physiol. Soc. Bethesda, MD 85, 5–34.

Samanipour, R., Maerefat, M., Nejad, H.R., 2013. Numerical study of the effect of ultrasound frequency on temperature distribution in layered tissue. J. Therm. Biol. Elsevier 38, 287–293.

Sapareto, S.A., Dewey, W.C., 1984. Thermal dose determination in cancer therapy. Int. J. Radiat. Oncol. Biol. Phys. Elsevier 10, 787–800.

Siauve, N., Nicolas, L., Vollaire, C., Marchal, C., 2004. Optimization of the sources in local hyperthermia using a combined finite element-genetic algorithm method. Int. J. Hyperth. Taylor Francis 20, 815–833.

Sklar, B., 1988. Digital Communications Fundamentals and Applications. published in. PTR Prentice Hall and.

Sofuni, A., Moriyasu, F., Sano, T., Itokawa, F., Tsuchiya, T., Kurihara, T., Ishii, K., Tsuji, S., Ikeuchi, N., Tanaka, R., 2014. Safety trial of high-intensity focused ultrasound therapy for pancreatic cancer. World J. Gastroenterol. WJG 20, 9570 Baishideng Publishing Group Inc.

Solovchuk, M.A., Sheu, T.W.H., Thiriet, M., 2012. Effects of acoustic nonlinearity and blood flow cooling during HIFU treatment. In: AIP Conf Proc AIP, pp. 83–88.

Solovchuk, M.A., Sheu, T.W.H., Thiriet, M., Lin, W.-L., 2013. On a computational study for investigating acoustic streaming and heating during focused ultrasound ablation of liver tumor. Appl. Therm. Eng. Elsevier 56, 62–76.

Solovchuk, M.A., Hwang, S.C., Chang, H., Thiriet, M., Sheu, T.W.H., 2014. Temperature elevation by HIFU in ex vivo porcine muscle: MRI measurement and simulation study. Med. Phys. Wiley Online Libr. 41.

Solovchuk, M., Sheu, T.W.-H., Thiriet, M., 2015. Multiphysics modeling of liver tumor ablation by high intensity focused ultrasound. Commun. Comput. Phys. Camb. Univ. Press 18, 1050–1071.

ter Haar, G., 2016. HIFU Tissue Ablation: Concept and Devices. Ther Ultrasound Springer, pp. 3–20.

Wang, S., Frenkel, V., Zderic, V., 2011. Optimization of pulsed focused ultrasound exposures for hyperthermia applications. J. Acoust. Soc. Am. ASA 130, 599–609.

Weidner, N., Semple, J.P., Welch, W.R., Folkman, J., 1991. Tumor angiogenesis and metastasis—correlation in invasive breast carcinoma. N. Engl. J. Med. Mass. Med. Soc. 324, 1–8.

Yacoob, S.M., Hassan, N.S., 2012. FDTD analysis of a noninvasive hyperthermia system for brain tumors. Biomed. Eng. Online BioMed. Central 11, 47.

Zhang, C.X., Zhang, Z., Chen, Y.Z., 2006. Effects of large blood vessel locations during high intensity focused ultrasound therapy for hepatic tumors: a finite element study. Eng. Med. Biol. Soc. 2005 IEEE-EMBS 2005 27th Annu. Int. Conf. IEEE 209–212.